An Open Annotated Dataset and Baseline Machine Learning Model for Segmentation of Vertebrae with Metastatic Bone Lesions from CT

Nazim Haouchine[2,3], David B. Hackney[1,3], Steve D. Pieper[4], William M. Wells III[2,3], Malika Sanhinova[1,3], Tracy A. Balboni[2,5], Alexander Spektor[2,5], Mai A. Huynh[2,5], David E. Kozono[2], Patrick Doyle[2,5], and Ron N. Alkalay[1,3]

1. Beth Israel Deaconess Medical Center, Boston, MA
2. Brigham and Women's Hospital, Boston, MA
3. Harvard Medical School, Boston, MA
4. Isomics, Inc., Cambridge, MA
5. Dana-Farber Cancer Institute., Boston, MA

Corresponding author(s): Ron N. Alkalay (rn_alkalay@bidmc.harvard.edu)

Abstract

Automatic analysis of pathologic vertebrae from computed tomography (CT) scans could significantly improve the diagnostic management of patients with metastatic spine disease. We provide the first publicly available annotated imaging dataset of cancerous CT spines to help develop artificial intelligence frameworks for automatic vertebrae segmentation and classification. This collection contains a dataset of 55 CT scans collected on patients with various types of primary cancers at two different institutions. In addition to raw images, data include manual segmentations and contours, vertebral level labeling, vertebral lesion-type classifications, and patient demographic details. Our automated segmentation model uses nnU-Net, a freely available open-source framework for deep learning in healthcare imaging, and is made publicly available. This data will facilitate the development and validation of models for predicting the mechanical response to loading and the resulting risk of fractures and spinal deformity.

Background & Summary

In 2022, it is estimated that there were more than 1.9 million new cancer cases in the United States (1). After the liver and the lungs, bones are the third most frequent target site of metastases (1), with the spine being the most frequent site of bone metastases (2, 3). Cancer patient autopsies (4) showed 73% of breast, 68% of prostate, and 35% of renal and lung subjects had vertebral bone metastases. Up to 50% of spinal metastases receive some form of treatment, and 5-10% receive surgical management (5, 6, 7). Patients are at high risk for skeletal adverse events, including bone pain, fracture, hypercalcemia, and neurological dysfunction secondary to the spinal cord or cauda equina compression (4, 9, 10, 11, 12), that may require palliative radiotherapy, surgery, or both. Skeletal adverse events profoundly and negatively impact patients' lives (13), causing disability and often requiring high doses of narcotics, causing reduced quality of life (14). They also increase psychological distress, decrease social functioning (15), and significantly impair normal function (16).

Although the impact of spinal metastasis on the vertebral column anatomical integrity is readily imaged with MRI and CT (17, 18, 19, 20, 21, 22, 23), in the absence of quantitative assessment (11, 24, 25, 26), standard-of-care imaging modalities (19, 27, 28, 29) do not provide precise estimates of the structural competence of the spine (17, 18, 19, 20, 21, 22, 23). This limited ability has a profound, negative impact on these patients' clinical care. Clinicians are forced to decide without objective quantitative criteria whether surgery or vertebral augmentation should be offered or withheld in attempts to treat to reduce the risk of fracture or to control pain. This can be particularly tragic when treatment could have been offered prior to the development of complications.

Implementing routine quantitative measurements from clinical imaging, such as vertebral segmentation, biomechanical quantification, lesion classification, and longitudinal growth monitoring, and estimates of

progression would therefore guide individualized earlier intervention. Several methods have been developed to computationally process CTs, radiographs or MRIs (CT being the most studied modality), and provide some such measurements (8,30). Recently, deep learning has been successfully applied to vertebral segmentation and classification tasks, demonstrating high accuracy and outperforming conventional methods (31). This success is due, in part, to the Large Scale Vertebrae Segmentation Challenge (VerSe) (32,33) where two datasets containing a total of 374 multi-detector CT scans with voxel level annotations were publically released. Before VerSe, only small public imaging datasets with vertebral segmentations existed (34,35,36,37,38,39), thereby hindering efforts by the medical image computing community to develop robust and accurate segmentation and classification methods. Nevertheless, one limitation of VerSe is the exclusion of scans with vertebral abnormalities such as bone metastasis and primary bone tumors from their dataset.

In this work, we provide the first publicly available imaging dataset of vertebral segmentation masks for spine CT images and annotations of vertebral lesions per vertebral level. This dataset is intended for large-scale deep learning aimed at automated spine segmentation, vertebral level, and lesion classification. These segmentations and classifications are expected to facilitate longitudinal studies for monitoring lesion growth and quantification of changes in vertebral mechanics that are associated with cancer-induced bone mechanical pain evolution or fracture. In current clinical practice, monitoring is subjective, labor-intensive, and variable and, to our knowledge, has no clinically-ready automated solution. Automated quantitation of vertebral mechanics would greatly aid in predicting fracture risk. In addition to the dataset, we also freely release the code and model weights for a trained deep learning model based on a recent convolutional neural network tool.

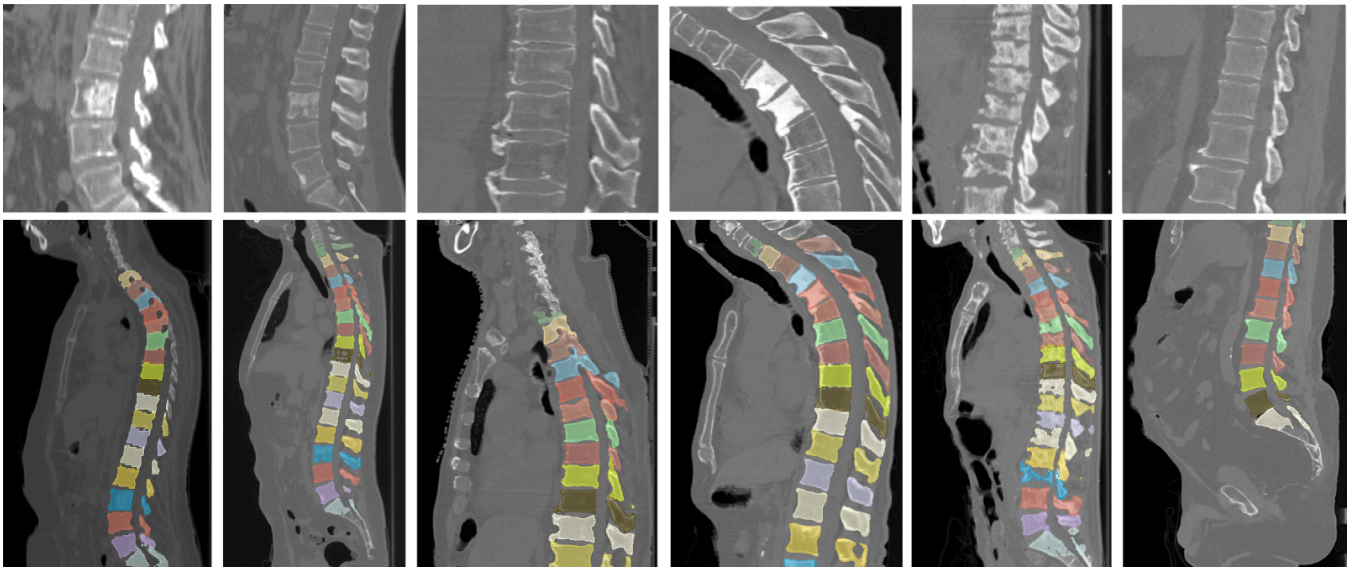

Figure 1: Example lesions and segmentations that can be found in the dataset. Top row: Spine CTs with lytic, blastic, and mixed lesions. Bottom row: Spine CTs with masks visualized as colored overlays.

Methods

Data overview:

This dataset contains a labeled dataset of 55 CT scans collected on 83 patients (Male:Female 36:19; mean age: 64.70, range: 33-82) with bone metastasis treated with radiotherapy at the Radiation Oncology Department at two institutions, Brigham and Women's Hospital (BWH) and Dana Farber Cancer Institute (DFCI). The CTs included in this dataset are of patients who received radiotherapy or Stereotactic Body Radiation Therapy (SBRT). In addition to the CT images, the dataset contains patient demographics data, primary cancer site, voxel-based segmentation of each vertebra, and vertebral lesion classification (not involved, blastic, lytic, and mixed). All structures were manually segmented and classified in consensus with the treating neuroradiologist.

The study cohort included all enrolled and eligible patients with documented spine metastases (CT, MR, or bone scan imaging) who were referred for radiation at DFCI between September 2020 and October 2021. This study does not include experimental radiation protocols and we expect our findings to be generalizable to patients treated at other institutions. Patients were identified for the study by the attending clinician according to the following inclusion criteria:

- Histologically or cytologically documented stage IV bone metastases and radiographic (CT scan or bone scan) evidence of bone metastases.
- Karnofsky Performance Status >70. This criterion was selected to enhance the likelihood of the patient participation to have sufficiently long survival to allow for the planned follow-up.

Patients were excluded if they had diseases of abnormal bone metabolism (including Paget disease, untreated hyperthyroidism, untreated hyperprolactinemia, and untreated Cushing disease) or had previously undergone surgery or vertebral augmentation at the site of radiation or adjacent levels. Patients with prior spinal RT were excluded only if the spinal region under consideration had undergone RT. Suitable patients were approached by the study research coordinator to inquire about their interest in participating in the study.

All contributions to this study were based on approval by Beth Israel Deaconess Medical Center (BIDMC), BWH, and DFCI Institutional Review Boards (IRB) and were conducted in accordance with the 1964 Declaration of Helsinki. Data were fully de-identified by removing all health information identifiers. Scans included no anatomy above the neck. All data were visually inspected before release. Because patients were selected retrospectively and the CT images were completely de-identified before analysis, informed consent from individual participants was not required for the study. In addition, the terms of the data sharing agreements were approved by the Office of Research and Academic Affairs at BIDMC.

Image acquisition

All images were obtained on a General Electric scanner (LightSpeed RT16), with the following acquisition (protocol) or a Siemens scanner (SOMATOM Confidence), with the following acquisition (Protocol). While acquisitions vary by patient, CT imaging was typically performed with in-plane resolution of 0.3125x0.3125mm, in-plane matrix of 512x512 and slice thickness of 1.0-1.5mm

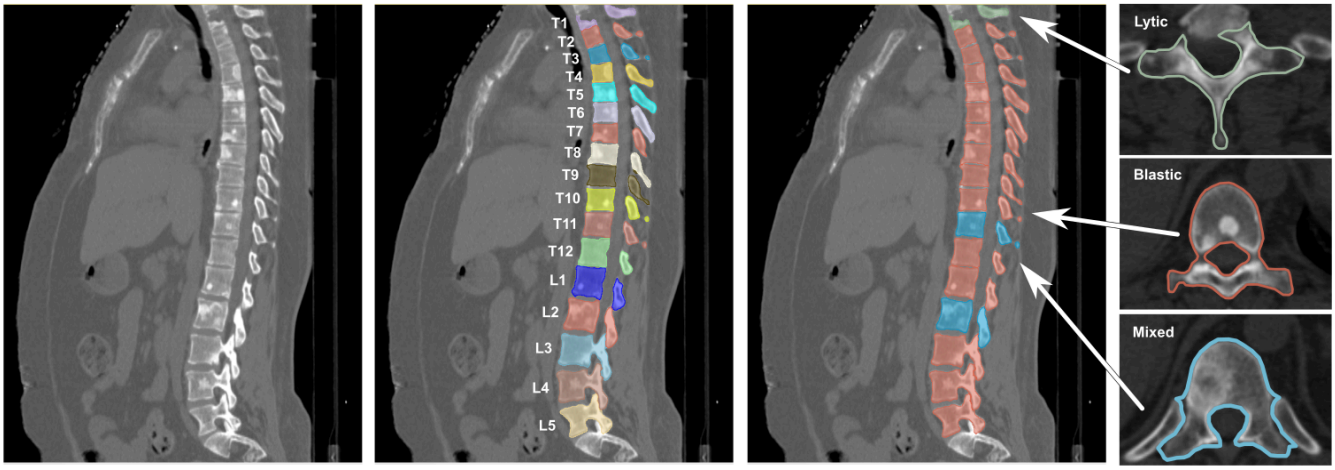

Figure 2: Illustrative example dataset of a patient with vertebral lesions with the raw CT, annotated segmentation and identification of vertebral levels, and lesion classification (Lytic, Blastic, and Mixed)

Vertebral segmentation, level annotation, and lesion classification

Following the acquisition of the CT scans, the images were imported into the 3D Slicer imaging software for manual segmentation. Manual segmentations were performed on the 55 spine CTs using an in-plane

semi-automated segmentation method by a radiologist and a biomechanical research engineer (DBH. and RNA), with 35 years and 25 years of experience, respectively. Using this software, delineation was performed on sequential 2D axial slices to produce 3D models for each structure. Voxel-level labels were thus generated as segmentation masks. Eighteen vertebrae (T1 to L5) were considered for annotation depending on the field of view, with labels from 6 to 25 in the original segmentation label maps. Note that partially visible vertebrae at the top or bottom of the scan (or both) were not annotated. In addition to the delineations, assessment of vertebral lesions was also performed. Vertebral body lesion type was classified as Not-involved, Lytic, Blastic, or Mixed. Figure 2 illustrates an example dataset of a patient.

Data transmission and de-identification

De-identified data was submitted to The Cancer Imaging Archive (TCIA) through its established selection and governance processes. The CT images exclude the head and, thus, any facial features.

Data Records

The images and associated files are publicly available on TCIA at:

https://doi.org/10.7937/kh36-ds04

The data are organized as illustrated in Figure 3. For each case, the CT image files are provided in DICOM format. The segmentation label map is also provided in DICOM format with one file including the entire multi-class labels. We provide the raw CT scans without any geometric modification, such as discretization, spatial transformation, or re-slicing. We used DCMQI (DICOM for Quantitative Imaging, https://qiicr.gitbook.io/dcmqi-guide) library to convert the segmentation masks from 3D Slicer NRRD format to DICOM, resulting in a standardized format compatible with TCIA requirements and interoperating with PACS and commercial tools. We followed the Systematized Nomenclature of Medicine Clinical Terms (SNOMED® CT, https://www.snomed.org/) coding scheme as the controlled terminology to label each vertebra. A file named *clinical_data.xls* that contains the lesion classification in Microsoft Excel format and maps every vertebra level for each scan with a lesion class is also provided.

In total, 55 patients were included, with 55 CT image series and 787 vertebrae encompassing 543 thoracic and 244 lumbar vertebrae. Among these vertebrae, 173 contain lesions, 111 thoracic and 72 lumbar, classified as 58 blastic, 54 lytic, and 61 mixed. This represents a considerable increase in available annotated data—particularly for lesion vertebrae—compared with previously available datasets (32,33,34,35,36,37,38,39).

```
Dataset
├── 10250/ -------------------------- De-identified Case ID
│   ├── 10250_CT/ ------------------- CT images in DICOM (1 image per slice)
│   │   ├── 000001.dcm ...
│   │   ├── 000002.dcm
│   │   └── ...
│   └── 10250_seg.dcm --------------- Segmentation masks in DICOM (1 file for all classes)
├── 10352/
│   ├── 10352_CT/
│   │   ├── 000001.dcm
│   │   ├── 000002.dcm
│   │   └── ...
│   └── 10352_seg.dcm
├── ...
└── clinical_data.xls
```

Figure 3: File structure.

Technical Validation: nnU-Net for Baseline Segmentation Performance

The quality of the images in this dataset and their segmentation masks were first assessed by radiologists through visual inspection of all cases using 3D Slicer.

For further validation, an automatic segmentation algorithm was trained and tested on the dataset. We trained a deep convolutional neural network using 55 spine CTs to segment the spine and outline the vertebrae from the background. Each vertebra is automatically localized and labeled, and 3D surfaces are generated using 3D Slicer. We used the nnU-Net framework (30), a self-adapting framework for 3D full-resolution image segmentation based on the U-Net architecture. We obtained an average segmentation accuracy of 94.33% ±2.24% Dice score on the spine CTs dataset not used in the training. Segmentation results on one patient are illustrated in Figure 4.

We then compared our model with the TotalSegmentator framework (31), trained on a spine CT dataset that excludes vertebral lesions. Our comparison exhibited an average improvement in Dice score of more than 3% over all spines and an average improvement in Dice score of more than 5% in vertebrae with bone metastasis, further validating the importance of our dataset.

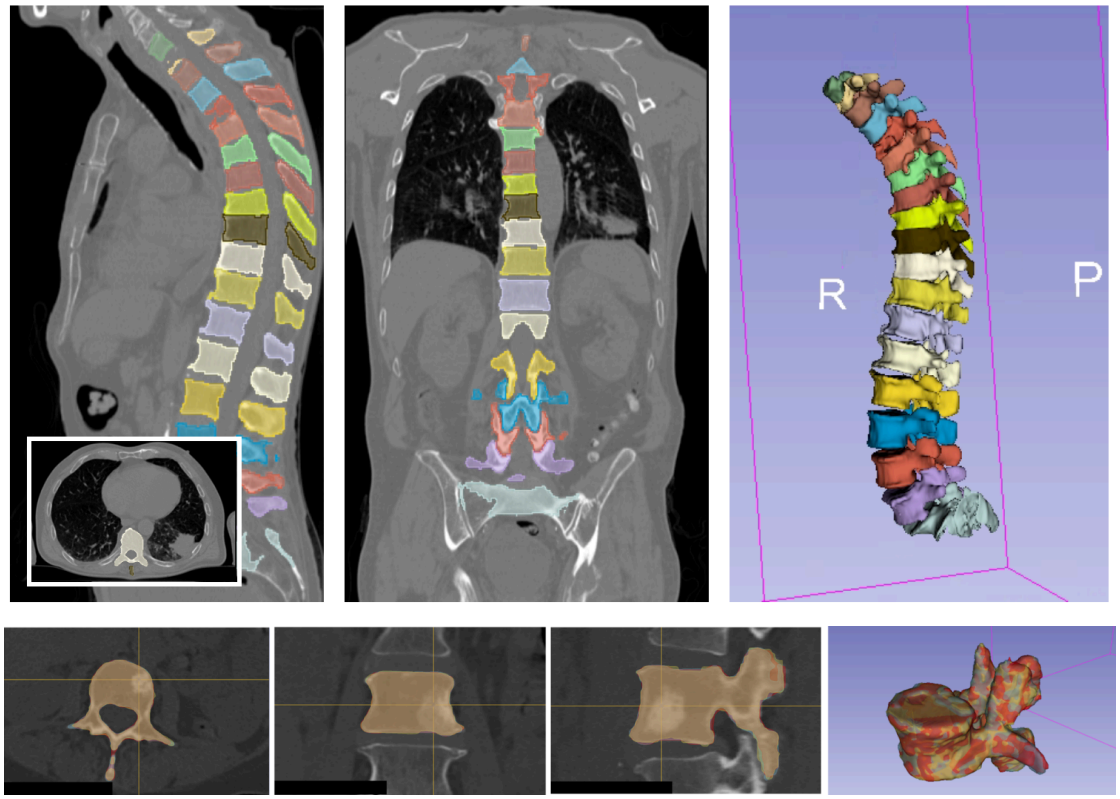

Figure 4: Segmentation results on one patient using the trained nnU-Net model. Top row: Axial, Coronal, Sagittal, and 3D views with segmentation masks. Bottom row: Segmentation results overlaid on ground truth annotation of one vertebra with a blastic lesion.

Usage Notes

We recommend 3D Slicer's DICOM viewer (https://www.slicer.org), a free and open-source platform for medical image informatics, image processing, and three-dimensional visualization to view the DICOM images. The CT images can be viewed without additional extensions. The segmentations can be viewed using the QuantitativeReporting extensions (https://qiicr.gitbook.io/quantitativereporting-guide/)

Acknowledgments
This work was supported by the NIAMS and the NIBIB of the National Institutes of Health under award numbers R01AR075964, 3R01AR075964-03S1, and K25EB035166.
We would like to thank Andrey Fedorov for his help with data conversion and formatting.

Competing interests
The authors declare no conflict of interest.

References

1. U.S. Cancer Statistics Working Group. U.S. Cancer Statistics Data Visualizations Tool. Cancer Facts & Figures 2022. In: Institute CfDCaPaNC, editor.: U.S. Department of Health and Human Services; 2022.

2. Roehrborn CG, Black Lk. The economic burden of prostate cancer. BJU Int. 2011;108(6):806-13. PubMed PMID: 21884356; PMCID: PMC Journal -- In Process.

3. Siegel R, DeSantis C, Virgo K, Stein K, Mariotto A, Smith T, Cooper D, Gansler T, Lerro C, Fedewa S, Lin C, Leach C, Cannady RS, Cho H, Scoppa S, Hachey M, Kirch R, Jemal A, Ward E. Cancer treatment and survivorship statistics, 2012. CA Cancer J Clin. 2012;62(4):220-41. PubMed PMID: 22700443; PMCID: PMC Journal - In Process.

4. Coleman RE. Metastatic bone disease: clinical features, pathophysiology and treatment strategies. Cancer Treat Rev. 2001;27(3):165-76

5. Bell GR. Surgical treatment of spinal tumors. Clin Orthop Relat Res. 1997;335:54-63

6. Bilsky MH, Lis E, Raizer J, Lee H, Boland P. The diagnosis and treatment of metastatic spinal tumor. Oncologist 1999;4(6):459-69. PubMed PMID: 10631690.

7. Walsh GL, Gokaslan ZL, McCutcheon IE, Mineo MT, Yasko AW, Swisher SG, Schrump DS, Nesbitt JC, Putnam JB, Jr., Roth JA. Anterior approaches to the thoracic spine in patients with cancer: indications and results. Ann Thorac Surg Oncol. 1977;64(6):1611-8,

8. Sanhinova M, Haouchine N, Pieper SD, Wells III WM, Balboni TA, Spektor A, Huynh MA, Guenette JP, Czajkowski B, Caplan S, Doyle P. Registration of longitudinal spine CTs for monitoring lesion growth. In Medical Imaging 2024: Image Processing 2024 Apr 2 (Vol. 12926, pp. 658-661). SPIE.

9. Bryson DJ, Wicks L, Ashford RU. The investigation and management of suspected malignant pathological fractures: a review for the general orthopaedic surgeon. Injury. 2015;46(10):1891 -9. PubMed PMID: 26254572; PMCID: PMC Journal -- In Process.

10. Lee SH, Tatsui CE, Ghia AJ, Amini B, Li J, Zavarella SM, Tannir NM, Brown PD, Rhines LD. Can the spinal instability neoplastic score prior to spinal radiosurgery predict compression fractures following stereotactic spinal radiosurgery for metastatic spinal tumor?: a post hoc analysis of prospective phase II single-institution trials. J Neurooncol. 2016;126(3):509-17. PubMed PMID: 26643804; PMCID: PMC JouRNAL - In Process.

11. Rose PS, Laufer I, Boland PJ, Hanover A, Bilsky MH, Yamada J, Lis E. Risk of fracture after single fraction image-guided intensity-modulated radiation therapy to spinal metastases. J Clin Oncol 2009;27(30):5075-9. PubMed PMID: 19738130; PMCID: PMC3664037.

12. Sahgal A, Whyne CM, Ma L, Larson DA, Fehlings MG. Vertebral compression fracture after stereotactic body radiotherapy for spinal metastases. Lancet Oncol 2013;14(8):e310-20. PubMed PMID: 23816297; PMCID: PMC Journal -- In Process.

13. Zhu XC, Zhang JL, Ge CT, Yu YY, Wang P, Yuan TF, Fu CY. Advances in cancer pain from bone metastasis. Drug Des Devel Ther. 2015;9:4239-45. Epub 2015/09/01. PubMed PMID: 26316696; PMCID: PMC4547660.

14. Rustoen T, Moum T, Padilla G, Paul S, Miaskowski C. Predictors of quality of life in oncology outpatients with pain from bone metastasis. J Pain Symptom Manage. 2005;30(3):234-42. Epub 2005/09/27. PubMed PMID: 16183007.

15. Coleman RE, Croucher PI, Padhani AR, Clezardin P, Chow E, Fallon M, Guise T, Colangeli S, Capanna R, Costa L. Bone metastases. Nat Rev Dis Primers. 2020;6(1):83. Epub 2020/10/17. PubMed PMID: 33060614.

16. Urch C. The pathophysiology of cancer-induced bone pain: current understanding. Palliat Med. 2004;18(4):267-74. Epub 2004/06/17. PubMed PMID: 15198116.

17. Algra PR, Bloem JL, Tissing H, Falke TH, Arndt JW, Verboom LJ. Detection of vertebral metastases: comparison between MR imaging and bone scintigraphy. Radiographics. 1991;11(2):219-32

18. Avrahami E, Tadmor R, Dally O, Hadar H. Early MR demonstration of spinal metastases in patients with normal radiographs and CT and radionuclide bone scans. J Comput Assist Tomogr. 1989;13(4):598-602

19. Matthay KK, Edeline V, Lumbroso J, Tanguy ML, Asselain B, Zucker JM, Valteau-Couanet D, Hartmann O, Michon J. Correlation of early metastatic response by 123I-metaiodobenzylguanidine scintigraphy with overall response and event-free survival in stage IV neuroblastoma. J Clin Oncol. 2003;21(13):2486-91

20. Saip P, Tenekeci N, Aydiner A, Dincer M, Inanc S, Demir C, Oral EN, Topuz E. Response evaluation of bone metastases in breast cancer: value of magnetic resonance imaging. Cancer Invest. 1999;17(8):575-80

21. Shin KH, Moon SH, Suh JS, Yang WI. Tumor volume change as a predictor of chemotherapeutic response in osteosarcoma. Clin Orthop. 2000(376):200-8

22. Carlson K, Astrom G, Nyman R, Ahlstrom H, Simonsson B. MR imaging of multiple myeloma in tumour mass measurement at diagnosis and during treatment. Acta Radiol. 1995;36(1):9-14

23. Ciray I, Lindman H, Astrom KG, Bergh J, Ahlstrom KH. Early response of breast cancer bone metastases to chemotherapy evaluated with MR imaging. Acta Radiol. 2001;42(2):198-206

24. Boehling NS, Grosshans DR, Allen PK, McAleer MF, Burton AW, Azeem S, Rhines LD, Chang EL. Vertebral compression fracture risk after stereotactic body radiotherapy for spinal metastases. J Neurosurg Spine. 2012;16(4):379-86. PubMed PMID: 22225488; PMCID: PMC Journal -- In Process.

25. Ejima Y, Matsuo Y, Sasaki R. The current status and future of radiotherapy for spinal bone metastases. J Orthop Sci. 2015;20(4):585-92. PubMed PMID: 25860575; PMCID: PMC3669258

26. Fourney DR, Frangou EM, Ryken TC, Dipaola CP, Shaffrey CI, Berven SH, Bilsky MH, Harrop JS, Fehlings MG, Boriani S, Chou D, Schmidt MH, Polly DW, Biagini R, Burch S, Dekutoski MB, Ganju A, Gerszten PC, Gokaslan ZL, Groff MW, Liebsch NJ, Mendel E, Okuno SH, Patel S, Rhines LD, Rose PS, Sciubba DM, Sundaresan N, Tomita K,

Varga PP, Vialle LR, Vrionis FD, Yamada Y, Fisher CG. Spinal instability neoplastic score: an analysis of reliability and validity from the spine oncology study group. J Clin Oncol. 2011;29(22):3072-7

27. Walls J, Bundred N, Howell A. Hypercalcemia and bone resorption in malignancy. Clin Orthop. 1995;312(51):51-63

28. Aizer-Dannon A, Bar-Am A, Ron IG, Flusser G, Even-Sapir E. Fused functional-anatomic images of metastatic cancer of cervix obtained by a combined gamma camera and an X-ray tube hybrid system with an illustrative case and review of the 18F-fluorodeoxyglucose literature. Gynecol Oncol. 2003;90(2):453-7

29. Roque M, Martinez M, Alonso P, Catala E, Garcia J, Ferrandiz M. Radioisotopes for metastatic bone pain. Cochrane Database Syst Rev. 2003;4:CD003347

30. Isensee, F., Jaeger, P. F., Kohl, S. A., Petersen, J., & Maier-Hein, K. H. (2021). nnU-Net: a self-configuring method for deep learning-based biomedical image segmentation. Nature methods, 18(2), 203-211.

31. Wasserthal J., Meyer M., Breit H., Cyriac J., Yang S., Segeroth M. TotalSegmentator: robust segmentation of 104 anatomical structures in CT images, 2022. URL: https://arxiv.org/abs/2208.05868. arXiv: 2208.05868

32. Löffler, Maximilian T., Anjany Sekuboyina, Alina Jacob, Anna-Lena Grau, Andreas Scharr, Malek El Husseini, Mareike Kallweit, Claus Zimmer, Thomas Baum, and Jan S. Kirschke. "A vertebral segmentation dataset with fracture grading." Radiology: Artificial Intelligence 2, no. 4 (2020): e190138.

33. Sekuboyina, Anjany, Malek E. Husseini, Amirhossein Bayat, Maximilian Löffler, Hans Liebl, Hongwei Li, Giles Tetteh et al. "VerSe: a vertebrae labelling and segmentation benchmark for multi-detector CT images." Medical image analysis 73 (2021): 102166.

34. Yao, J., Burns, J. E., Munoz, H., & Summers, R. M. (2012). Detection of vertebral body fractures based on cortical shell unwrapping. In International Conference on Medical Image Computing and Computer-Assisted Intervention (pp. 509–516). Springer.

35. Yao, J., Burns, J. E., Forsberg, D., Seitel, A., Rasoulian, A., Abolmaesumi, P., Hammernik, K., Urschler, M., Ibragimov, B., Korez, R., Vrtovec, T., Castro-Mateos, I., Pozo, J. M., Frangi, A. F., Summers, R. M., & Li, S. (2016). A multi-center milestone study of clinical vertebral ct segmentation. Computerized Medical Imaging and Graphics, 49, 16 – 28.

36. Korez, R., Ibragimov, B., Likar, B., Pernuˇs, F., & Vrtovec, T. (2015). A framework for automated spine and vertebrae interpolation-based detection and model-based segmentation. IEEE transactions on medical imaging, 34, 1649–1662.

37. Korez, R., Likar, B., Pernus, F., & Vrtovec, T. (2016). Model-based segmentation of vertebral bodies from MR images with 3d CNNs. In International conference on medical image computing and computer-assisted intervention (pp. 433–441). Springer.

38. Ibragimov, B., Likar, B., Pernus, F., & Vrtovec, T. (2014). Shape representation for efficient landmark-based segmentation in 3-d. IEEE Transactions on Medical Imaging, 33, 861–874.

39. Glocker, B., Zikic, D., Konukoglu, E., Haynor, D. R., & Criminisi, A. (2013). Vertebrae localization in pathological spine CT via dense classification from sparse annotations. In International conference on medical image computing and computer-assisted intervention (pp. 262–270). Springer.